MACHINE LEARNING AND MOLECULAR DYNAMICS SIMULATIONS OF THERMAL TRANSPORT

by

Adam S.G. Garrett

A Thesis

Submitted to the Faculty of Purdue University

In Partial Fulfillment of the Requirements for the degree of

Master of Science in Mechanical Engineering

School of Mechanical Engineering

West Lafayette, Indiana

August 2021

THE PURDUE UNIVERSITY GRADUATE SCHOOL
STATEMENT OF COMMITTEE APPROVAL

Dr. Xiulin Ruan, Chair
School of Mechanical Engineering

Dr. Amy Marconnet
School of Mechanical Engineering

Dr. Guang Lin
School of Mathematics/Mechanical Engineering

Approved by:
Dr. Nicole Key

Dedicated to my parent Ron and Eva Garrett for their unwavering support through my academic career.

ACKNOWLEDGMENTS

I would like to thank Dr. Xiulin Ruan for his support over the years. Starting in 2018 as an undergraduate researcher, Professor Ruan has helped guide me through my development as a researcher. I would also like to thank Dr. Chowdhurry for his guidance and support. Dr. Chowdhurry served as a valuable mentor to me from my first day with the group up until now. Finally, I would like to thank my committee members Dr. Amy Marconnet and Dr. Guang Lin for their support, as well as all the members of the Nanoscale Energy Transport and Conversion Laboratory.

TABLE OF CONTENTS

LIST OF FIGURES

ABSTRACT

The need for sources of efficient and renewable energy has become an issue of great importance in recent years. Fossil fuels are diminishing in supply, and they not only pollute the environment, but have also proven to be inefficient in many cases, losing a large portion of the total energy generated to waste heat, instead of usable energy.

The first work this thesis addresses is the development of a Genetic Algorithm (GA) optimization method for the search and discovery of semiconductor materials for use in thermoelectric devices. The specific material in question is the Silicon Germanium superlattice. This structure made of alternating layers of Si and Ge is known to be one of the better materials for thermoelectric energy generation at elevated temperature, along with Bismuth-Telluride that targets room temperature. Previously, it has been shown that random multilayer (RML) structures can lower thermal conductivity as compared to periodic superlattices due to phonon localization. However, it was unknown which specific RML would yield the lowest thermal conductivity, due to the large design space from which these RML's can be generated. Considering this, a global and non-smooth optimization method was employed to search for the best possible structure. Results not only showed that the thermal conductivity could be lowered even further, but that there was an optimal average period for the RML's that produced the best results.

The second work discussed in this thesis concerns itself with the development of a Neural Network Potential (NNP) for use in Molecular Dynamics (MD) simulations. There are multiple methods for running MD including *ab-initio* methods such as Density Functional Theory (DFT) calculations and classical MD with the use of empirical potentials. Unfortunately, DFT is too time consuming for systems larger than a few hundred atoms, and empirical potentials can be inaccurate. Therefore, a NNP for bulk Silicon trained on DFT was developed, and it was shown that the phonon dispersion for Si could be accurately reproduced.

1. INTRODUCTION

1.1 Thermal Transport in RML's and Si

When discussing thermal transport in this thesis we are concerned with heat conduction as opposed to convection and radiation. To be more specific, we are concerned with thermal transport through semiconductor solids at the nanoscale. The primary heat carrier at this level is the phonon, defined as the quantum of energy for lattice vibrations [1]. When analyzing a structure's thermal property at the nanoscale it is important to take phonon properties such as scattering and dispersion into consideration.

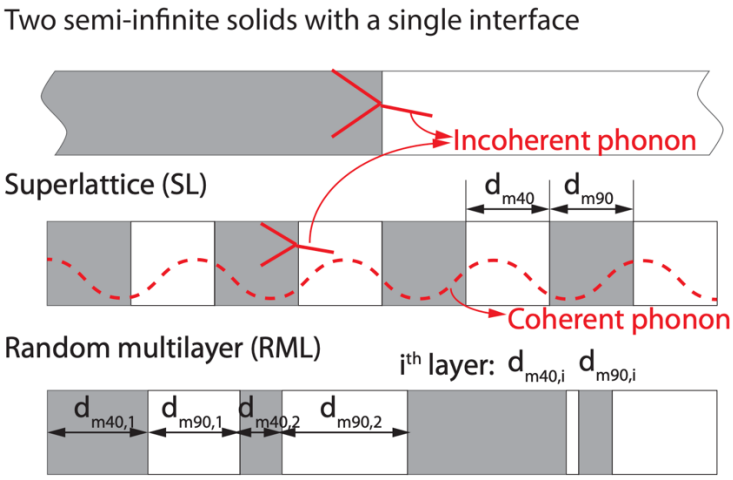

Figure 1.1: Phonon transport through different superlattice configurations [2]

It has been proposed that making the layer thickness random in a periodic superlattice could lower the thermal conductivity and potentially enhance thermoelectric energy conversion efficiency [2]. The design of RML structures is primarily concerned with phonon scattering. To help illustrate this point, consider microwaves and radio waves. Comparing these two, they are on vastly different orders of magnitude in terms of wavelengths. Consider that when a microwave device is operated, the microwaves are contained within the device and will not leak, however, a radio wave with its much larger wavelength will pass right through a microwave oven, car, and even house walls. Now let us extrapolate this idea to phonon transport through RML structures. Figure 1.1 shows a schematic of phonon transport through different multilayer types. Notice that

the coherent phonons can pass through the different interfaces as if they are not there, while the shorter wavelength phonons, which do see the interface, are scattered. This scattering is what allows for significant reduction in the thermal conductivity of superlattices. However, the coherent phonons are still not scattered. To further reduce the thermal conductivity, RML's can be used as the variation in layer thickness allows for localization of coherent phonons, hence phonons of multiple wavelengths are now all scattered.

Although Silicon is used in conjunction with Ge for RML studies, it is also an important material on its own. Silicon is widely used in the electronics industry for two main reasons: it is a good semiconductor, and it is readily available [3]. Since Si is used so widely in electronics, its thermal properties are also of great importance. Without proper thermal management, many of today's electronics would not functional properly due to overheating. Understanding the thermal properties of Silicon is necessary for the continued development and improvement of electronic devices.

1.2 Molecular Dynamics

1.2.1 Classical MD

Molecular dynamics is a method of simulating atomic structures by solving $F = ma$ at multiple timesteps throughout the simulation region to extract atomic energies, and from that other structural and material properties. For this study, the Large-scale Atomic/Molecular Massively Parallel Simulator (LAMMPS) was used to carry out MD runs [4]. The use of this program as with any MD package or code required the use of an interatomic potential to describe the interactions between atoms. A basic type of potential is the Leonard-Jones 2-Body potential which can be seen in Figure 1.2. These potentials define the energy of atomic interactions as a function of system parameters. For the LJ case, only the distance between two atoms is considered, however other potentials can include contributions between multiple atoms as well as angular data. For Silicon, one of the most widely accepted potentials is the Tersoff many-body potential, which was used in this study for comparison [5]. For Aluminum as well as the interface system the modified embedded atom method (MEAM) potential was used for comparison and structure generation before DFT [6].

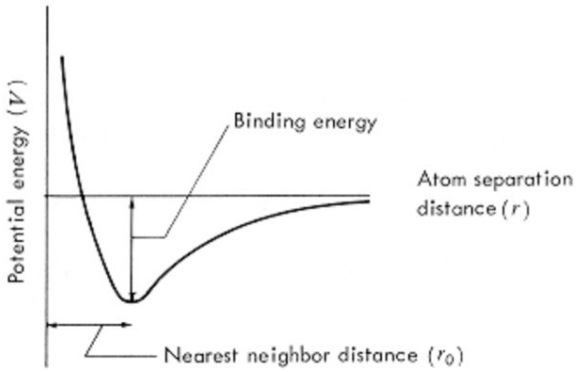

Figure 1.2: 2-Body Leonard Jones Potential [7]

These potentials are developed by fitting experimental and DFT data to an appropriate functional form. This method allows for molecular dynamics to be run at greater efficiency and speed compared to DFT and experiment. However, there is a trade off in accuracy. For example, the Si Tersoff potential tends to overestimate thermal conductivity values [8]. The experimental thermal conductivity for Silicon at 500K is reported to be approximately 80 W/mK, however the Tersoff potential reports values closer to 120 W/mK [8]. The functions describing the Tersoff potential, for example, can be seen in Figure 1.3. Here f_r represents the two body interactions and f_a represents the three body interactions [9].

$$
\begin{aligned}
E &= \frac{1}{2}\sum_i \sum_{j\neq i} V_{ij} \\
V_{ij} &= f_C(r_{ij}+\delta)\left[f_R(r_{ij}+\delta) + b_{ij} f_A(r_{ij}+\delta)\right] \\
f_C(r) &= \begin{cases} 1 & r < R-D \\ \frac{1}{2} - \frac{1}{2}\sin\left(\frac{\pi}{2}\frac{r-R}{D}\right) & R-D < r < R+D \\ 0 & r > R+D \end{cases} \\
f_R(r) &= A\exp(-\lambda_1 r) \\
f_A(r) &= -B\exp(-\lambda_2 r) \\
b_{ij} &= (1+\beta^n {\zeta_{ij}}^n)^{-\frac{1}{2n}} \\
\zeta_{ij} &= \sum_{k\neq i,j} f_C(r_{ik}+\delta) g\left[\theta_{ijk}(r_{ij}, r_{ik})\right] \exp\left[{\lambda_3}^m (r_{ij}-r_{ik})^m\right] \\
g(\theta) &= \gamma_{ijk}\left(1 + \frac{c^2}{d^2} - \frac{c^2}{\left[d^2 + (\cos\theta - \cos\theta_0)^2\right]}\right)
\end{aligned}
$$

Figure 1.3: Functional form of Tersoff potential [9].

1.2.2 EMD vs NEMD

EMD (Equilibrium Molecular Dynamics) and NEMD (Non-Equilibrium Molecular Dynamics) are two well-known methods for calculating thermal conductivity with molecular dynamics. EMD employs the use of the Green-Kubo method. The heat flux is found using equation 1 and, from there thermal conductivity is calculated using equation 2, which is the autocorrelation of the heat flux to thermal conductivity [10].

$$\boldsymbol{J} = \frac{1}{V}\left[\sum_i e_i \boldsymbol{v_i} + \frac{1}{2}\sum_{i<j}\left(\boldsymbol{F_{ij}} \cdot \left(\boldsymbol{v_i} + \boldsymbol{v_j}\right)\right)\boldsymbol{r_{ij}}\right] \quad (1)$$

$$k = \frac{V}{3k_B T^2}\int_0^\infty \langle \boldsymbol{J}(0) \cdot \boldsymbol{J}(t)\rangle dt \quad (2)$$

where *J* is heat flux, *e* is per atom energy, *r* is distance, *v* is velocity, *F* is force, *V* is volume, and *kb* is the Boltzmann constant. However, this method usually comes with considerable uncertainty, and requires long MD production runs to produce viable data [11].

Therefore, NEMD was used for thermal conductivity calculations. This method is more straightforward, as it imposes a temperature gradient on a system, calculates the energy being transferred through the system, and then employs Fourier's Law, as seen in.

$$q_x = -kA\frac{dT}{dx} \quad (3)$$

Figure 1.4 shows a plot of a system that has had a temperature gradient imposed with the calculated slope drawn over the plot. The very ends of the simulation domain must be kept in place for this simulation to work. The temperature gradient is imposed by fixing a constant temperature on both ends of the simulation box. With this temperature gradient imposed, the system is allowed to run under NVE (constant number of particles, volume, and energy) conditions, and the resultant temperature gradient is allowed to develop in the middle section, which is the section to be analyzed. Energy is calculated as the average of energy being added to the hot region and subtracted from the cold, which should be of approximately equal magnitudes. The temperature gradient is acquired by fitting a line to the middle section and retrieving the slope.

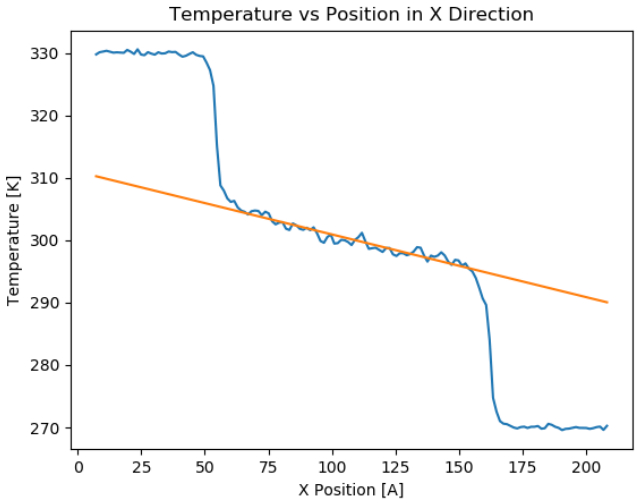

Figure 1.4: Temperature gradient for NEMD simulation of Silicon.

1.3 Genetic Algorithm

1.3.1 Algorithm

To address the extremely large design space, we explore the genetic algorithm in this work. The genetic algorithm is a global and non-smooth optimization method that can also be considered a machine learning algorithm. This method mimics natural evolution by encoding the chosen design variables into binary (each 0 or 1 is a 'gene') to form a string or 'chromosome'. This process is repeated for multiple random initial design values until a set of designs, or a 'population', is generated. Each member of the population then has its fitness evaluated by running the chosen designs through the objective function and constraint functions to check its performance. Then the members with the highest fitness are chosen to generate the next population. Fitness is characterized by a design's performance with the objective function and the constraint functions, with the goal being to minimize the objective and to not violate the constraints. The next population is generated by applying two actions to the parents: cross-over and mutation. 'Cross over' means to split each structure at a certain point and swap the sections to generate two new structures. 'Mutation' involves picking one or more individual genes and switching their value. These processes are visualized in Figure 1.5. Finally, the best performing chromosome of each generation is saved and updated as needed. Every other generation or so, one or two completely random structures may be introduced as well to increase the algorithm's global performance.

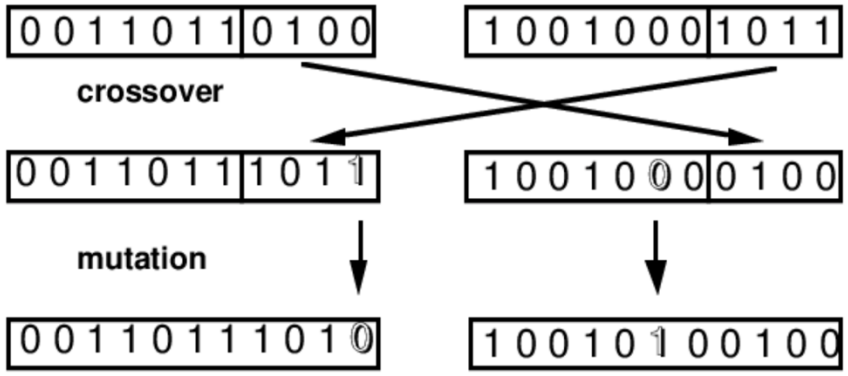

Figure 1.5: Visualization for cross-over and mutation processes in GA [12].

The Genetic Algorithm requires little input from the user other than the starting designs and rates for mutation and cross over. Since the GA is global and non-smooth, the initial choice of design should not be a major factor in the outcome of the final designs. The values for mutation and cross over rate may be chosen at the user's discretion as well, depending on the magnitude of variation desired from generation to generation.

1.4 Machine Learning Potential

1.4.1 Types of MLP's

Machine Learning Potential (MLP) refers to interatomic potential that is derived with or uses any form of machine learning methods. Two of the more common methods are Gaussian Approximation Potentials (GAP) and Neural Network Potentials (NNP). The GAP method was implemented by Bartok et. al, and has been successfully used to produce a GAP for graphene [13][14]. Meanwhile, neural networks as a form of machine learning, and machine learning potential, have been around for some time but were greatly improved upon by the works of Behler and Parrinello which will be discussed shortly. For this study, the focus will remain on NNP's.

1.4.2 Neural Network Potentials

Neural Networks

Neural networks are a form of supervised machine learning where a computer attempts to learn from data and make predictions. Neural networks accomplish this by creating a network of 'neurons' made up of layers of interconnected nodes which are meant to mimic organic thought processes. A schematic of a basic neural network can be seen in Figure 1.6. We see that a network is formed by each input layer sending data to each corresponding output layer. For example, the hidden layers in the diagram each receive data from the inputs multiplied by a certain weight. The weights serve to assign importance to the data. For example, were this a neural network meant for classification, data that better captured differences and helped in classification would receive a higher weight. This data is then passed through an activation function at the receiver node. The purpose of this is to eliminate linearity in the network and control the flow of information. Without an activation function a neural network is just a system of linear equations, and therefore only provides a linear regression model [15]. The model is trained by tuning the weights and bias values as the model learns to identify certain features that aid in classification.

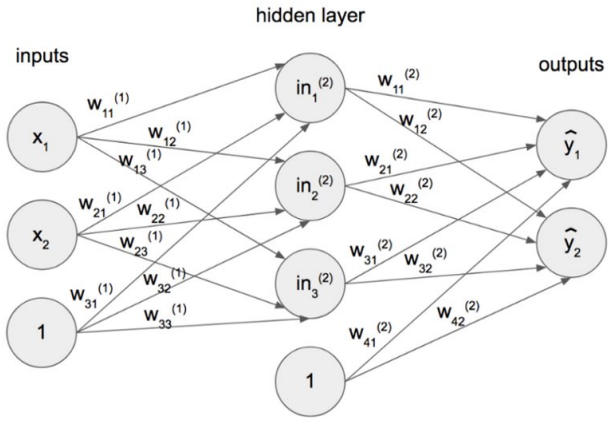

Figure 1.6: General representation of a neural network [17]

Implementation for Potential

The goal is to use a neural network as an interatomic potential. However, this introduces some issues when using the neural network structure displayed above. The input for a NNP is

atomic positions. The error here arises from a form of 'double dipping'. For example, if we have a system of 3 atoms of the same type, say atoms i, j, and k, then the system i-j-k will return a certain energy value. Now, if we take this same system but change the position of two atoms, say we have j-i-k, we have the same exact system. Unfortunately, the NNP will not see it this way, but will recognize this as an entirely new system, and it is possible it could get assigned a different energy value than it was assigned previously. To avoid this problem, Behler proposed a set of atom-centered symmetry functions that would instead define local atomic environments instead of specific atom positions. The goal of these functions is to eliminate variance in system energy if that system were to have atom coordinates switched, or if the system were to be rotated or translated [15]. Examples of radial and angular symmetry functions can be seen in equations 4 and 5 [15].

$$G_i = \sum_j \cos\left(kR_{ij}\right) \cdot f_c(R_{ij}) \quad \text{where} \quad f_c\left(R_{ij}\right) = \begin{cases} 0.5\left[\cos\left(\frac{\pi R_{ij}}{R_c}\right) + 1\right] for\ R_{ij} \le R_c \\ 0\ for\ R_{ij} > R_c \end{cases} \tag{4}$$

$$G_i = 2^{1-\zeta} \sum_{j,k\neq i}^{all} (1 + \lambda \cos^{\zeta}\left(\Theta_{ijk}\right) \cdot e^{-\eta\left(R_{ij}^2 + R_{ik}^2\right)} \cdot f_c(R_{ij}) \cdot f_c(R_{ik}) \tag{5}$$

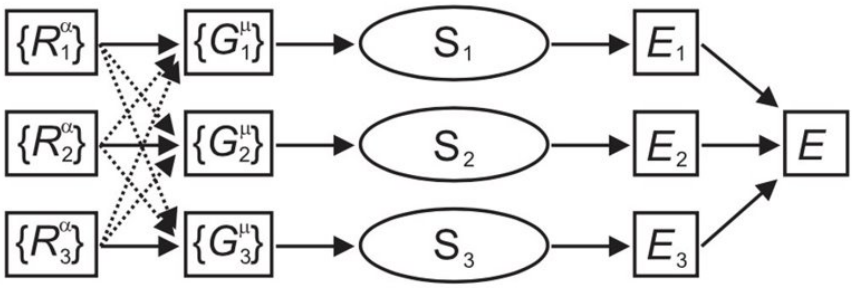

Figure 1.7: Neural network recommended by Behler and Parrinello for NNP [16].

Behler and Parrinello, along with their suggestions on using symmetry functions to convert the inputs, also proposed a slightly altered form for the neural network. This network, shown in Figure 1.7, shows the conversion of Cartesian coordinates into symmetry functions,

followed by sub neural networks for each atom, which gives the contribution of that atom to the total energy, and finally the summation of each atom into the total system energy [16]. While these methods are well regarded by many, and implemented in this work as well, it is worth noting that there is flexibility in choosing inputs for NNP's. For example, Sanville et. al successfully produced a NNP for bulk silicon using a slightly different method. Instead of passing the cartesian coordinates of the atoms through symmetry functions, the network is set up to take a variable number of inputs for each atom, and the complete geometric environment of each atom is described [18]. Each input is a vector which corresponds to a chain of 5 atoms, and each vector has 13 variables corresponding to different features of that 5-atom chain [18]. Figure 1.8 shows a schematic depicting the possible input variables.

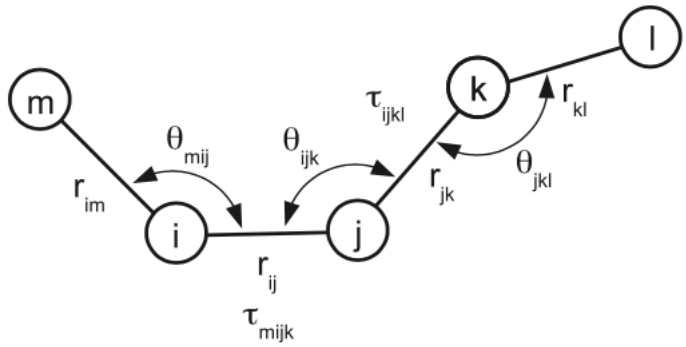

Figure 1.8: NNP input method employed by Sanville [18].

Finally, we mention DeePMD kit, which is a deep learning package meant to assist in the development of Neural Network Potentials. DeePMD-kit is a package to train many-body potentials for molecular dynamics simulations, that has been interfaced with TensorFlow and LAMMPS. The energy for the system is constructed the same as in the Behler and Parrinello framework where the total energy is a summation of the contributions of individual atoms [16]. The energy of each individual atom is dependent on its local atomic environment which includes all the surrounding atoms contained within the chosen cutoff radius. This framework offers a third alternative to describing the inputs for the neural network that is discussed in detail in Ref.

[20]. DeePMD can be trained on VASP output data directly if the OUTCAR file is provided. From VASP the model is trained on the system box coordinates, atom positions, system energy, force, and virial. Once training is complete the output model can easily be interfaced with numerous MD programs including LAMMPS, NAMD, and i-PI [19].

2. DESIGN FOR ULTRA-LOW THERMAL CONDUCTIVITY RANDOM MULTILAYER STRUCTURES

2.1 Motivation/Overview

Currently, 84% of the worlds energy still comes from fossil fuels [21]. With energy costs rising, fossil fuels being depleted, and pollution levels rising, it is important to consider and further advance research into alternative energy generation methods. Approximately 70% of energy generated by humans is lost to the ambient environment as waste heat [22]. One method of energy generation that serves as a renewable energy method while increasing the efficiency of current methods is thermoelectric energy generation. Thermoelectric devices such as the one shown in Figure 2.1 are made up of rows of semiconductor materials alternating between 'n' and 'p' types. When a temperature gradient is applied to this device, a current is formed, this is defined as the thermoelectric effect [23]. The efficiency of these devices is measured using figure of merit, or zT,

$$zT = \frac{S^2}{\rho k} T \qquad (6)$$

where S is the Seebeck coefficient, ρ is electrical resistivity, k is thermal conductivity, and T is temperature [24]. Therefore, to achieve a high figure of merit (maximize zT), thermal conductivity should be as low as possible.

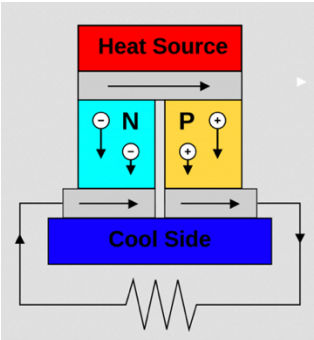

Figure 2.1: Schematic of thermoelectric energy generation device [23].

2.2 GA Implementation

The general framework for a GA has already been given, here the specific implementation of the GA for this study will be discussed. Unlike regular GA, there are not multiple design variables to encode into binary. Instead, the superlattice structures themselves were the design variables. Since the structures only display the RML in one dimension, each layer of Si was coded to '1' and each layer of Ge coded to '2'. With this, each chromosome for the GA was a series of 1's and 2's, where each gene corresponded to one of the materials. Cross over and mutation were employed normally. The final change from a typical GA was the choice of objective function. In this case, there was not an actual function that could describe the thermal conductivity, instead, Molecular Dynamics simulations served as the objective function.

The calculation of thermal conductivity for each structure was done using NEMD implemented in LAMMPS. The ends of the simulation box were fixed, and the entire region split into 3 regions of 40 atomic layers each. The middle region held the actual RML, while the ends were defined as either bulk Si or Ge thermostatted. System equilibration was done at both NVT (constant particles, volume, and temperature) and NPT (constant particles, pressure, and temperature) ensembles before the production run. Production runs were completed with an NVE fix for the RML, and Langevin thermostat fixes for the thermostatted regions [25]. Thermal conductivity was calculated using Fourier's Law, with temperature gradient and energy values being calculated as described in section 1. Then, as in any optimization, the goal was to lower the thermal conductivity, so structures reporting the lowest thermal conductivity were deemed best and used to generate the next generation. A sample NEMD input script can be found in Appendix B, and Figure 2.2 shows a visual of the GA.

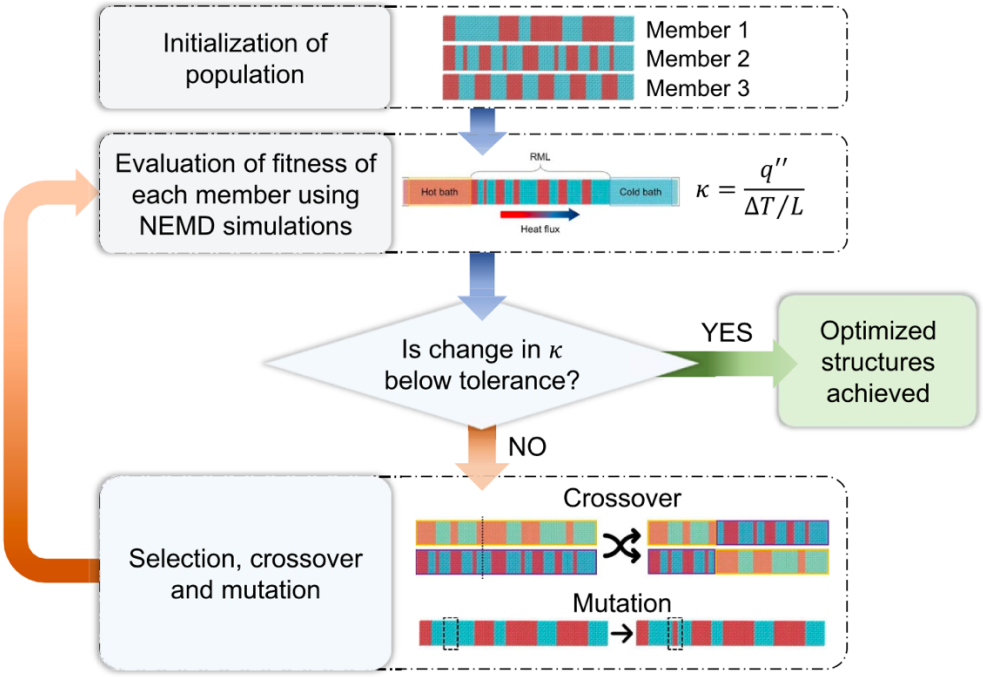

Figure 2.2: Graphical representation of Genetic Algorithm for RML design [26].

2.3 Tool Development

Part of the work on the GA involved publishing it as a simulation tool to nanoHub.org. This work involved interfacing the GA written in python with the Rappture toolkit used by nanoHub to generate graphical user interfaces (GUI) for simulation tools. Since the RML extends in the z-direction, the user can set the x-y dimensions (cross sectional area), RML length, and the lattice constants of the two materials to be used. The GA specific settings that can be set by the user are generations and populations. The GUI can be seen in Figure 2.3 [27].

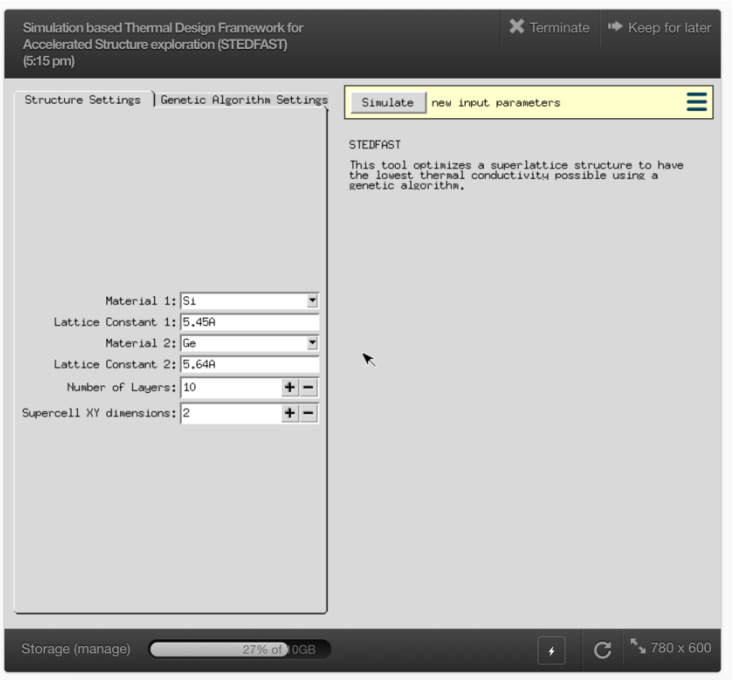

Figure 2.3: GUI for GA tool (STEDFAST) [27].

2.4 Results and Discussion

It can be shown that periodic Si-Ge superlattice structures achieve an absolute minimum thermal conductivity of 3.5 W/mK at a period of approximately 4.5 nm, where the period is defined as the length of a Si-Ge pair in the structure. Also, we can show that this lower limit can be broken with a random multilayer structure. However, due to the large design space and inefficient nature of manual RML search, the GA was employed in the search for better performing structures [26].

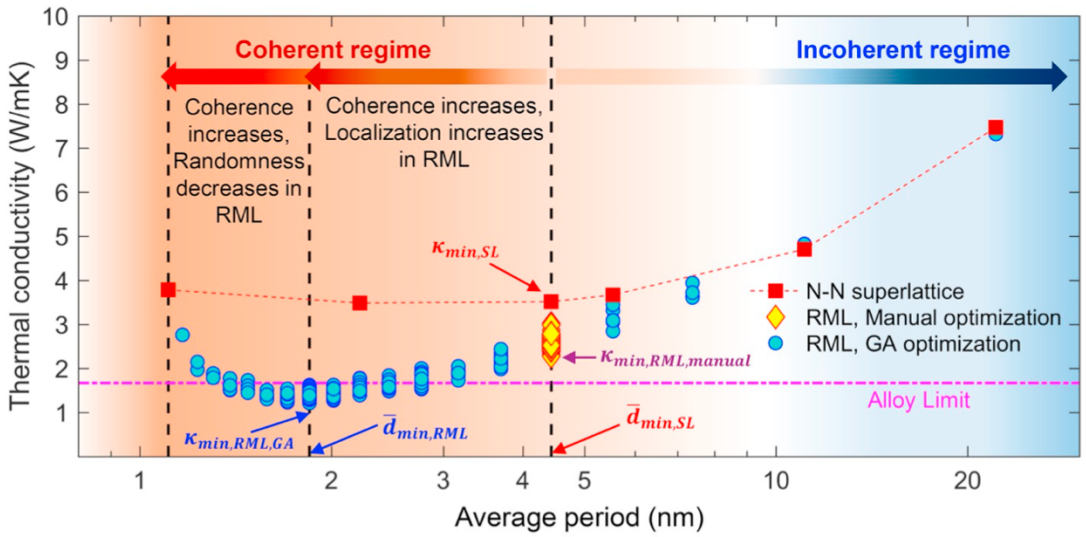

Figure 2.4: Thermal conductivity plotted against average RML period [26].

The results of the Genetic Algorithm optimization showed that not only could the superlattice structure minimum thermal conductivity be broken even further than the manual RML search, but it also showed an interesting convergence when it came to one of the features of the RML. Figure 2.4 shows that a minimum thermal conductivity of approximately 1 W/mK is achieved at an average period length of 1.85 nm, far below the original superlattice minimum of 3.5 W/mK. There is also a noticeable trend in the thermal conductivity values versus the average period length. Where the previous minimum for superlattice structures and RML structures found manually was approximately 3.5 nm, this shows the optimum average period length is much lower at 1.85 nm [26].

Figure 2.5: Best RML structure from GA. Corresponds to 1.85 nm average period [26].

The reason for this minimum has to do with the phonon scattering at the interfaces. Figure 2.5 shows the structure that achieved the lowest thermal conductivity from the GA. This structure has maximized the number of interfaces it can contain without becoming a 1-1 or 2-2 superlattice, which some structures at lower average period did. This allows for the maximum amount of

phonon localization to occur such that many coherent phonons cannot pass through the structure, thus efficiently reducing thermal conductivity.

3. NEURAL NETWORK POTENTIAL FOR PHONON PROPERTIES AND THERMAL CONDUCTIVITY OF SILICON

3.1 Motivation/Overview

The purpose of using Molecular Dynamics to study systems is that it can give us insights into the underlying physics in ways that theory and experiment cannot. The previous study on the GA used MD as an objective function to analyze thermal conductivity of SiGe superlattices. However, how accurate are those results? A study by Cruz et al. showed that thermal conductivity of Silicon when calculated using the Tersoff potential, is much higher than what is reported in experiment. To be more precise, Tersoff reports 120 W/mK at 500K while experiment reports just 80 W/mK [8]. Therefore, molecular dynamics based on empirical potentials can often only be used to explore the trends rather than quantitative comparison with experiments.

Silicon plays an important role in the electronics industry. Even the previous study regarding the GA was heavily dependent on Silicon. Therefore, an accurate computational model of Silicon without the expenses of DFT is needed. This study shows the development and testing of a Neural Network Potential for bulk Silicon. The goal of this potential is to have the process repeated for bulk Aluminum, and finally the Si-Al interface, another system commonly found in microelectronics.

3.2 Data Generation

When preparing a neural network for any application the training data is the first and most important step in the process. In the case of a neural network potential, the potential will only perform molecular dynamics to the accuracy of the method chosen to generate the data. For this reason, if we want the model to perform with the accuracy of experiment or first principles calculations, then the data needs to be generated with those methods respectively. For this study, molecular dynamics using Density Functional Theory (DFT) was chosen for data generation and implemented using the Vienna Ab-initio Simulation Package (VASP) [28]. Simulations were initially run under constant pressure and temperature (NPT) conditions for 500 timesteps. This process was repeated for 5 temperatures ranging from 100 to 500 Kelvin. Each temperature had 5 equilibration runs, which then led to 20 production runs starting from each equilibrated system.

With this data, the phonon dispersion curves for Silicon were reproduced successfully. However, the thermal conductivity was underestimated. Therefore, to improve the accuracy the data was generated anew, this time using a finer mesh grid of 4 x 4 x 4 as opposed to 3 x 3 x 3 previously. To account for the increase in simulation time each simulation was only run for 250 timesteps instead of 500.

3.3 Neural Network

The neural network potential file was generated using the DeePMD package, a code written in python, C++, and TensorFlow to generate potentials given data [19]. The important model parameters such as cutoff type, cutoff radius, smooth distance, number of layers and nodes, and activation function could be set in the input file. Based on previous literature the initial model was set to 3 layers, with 30 nodes each as a starting point, and the tanh activation function selected [29]. The other parameters were chosen as follows: 5 hidden layers with 120 nodes each, smooth cutoff, cutoff of 5 angstroms smoothed out to 5.4 angstroms.

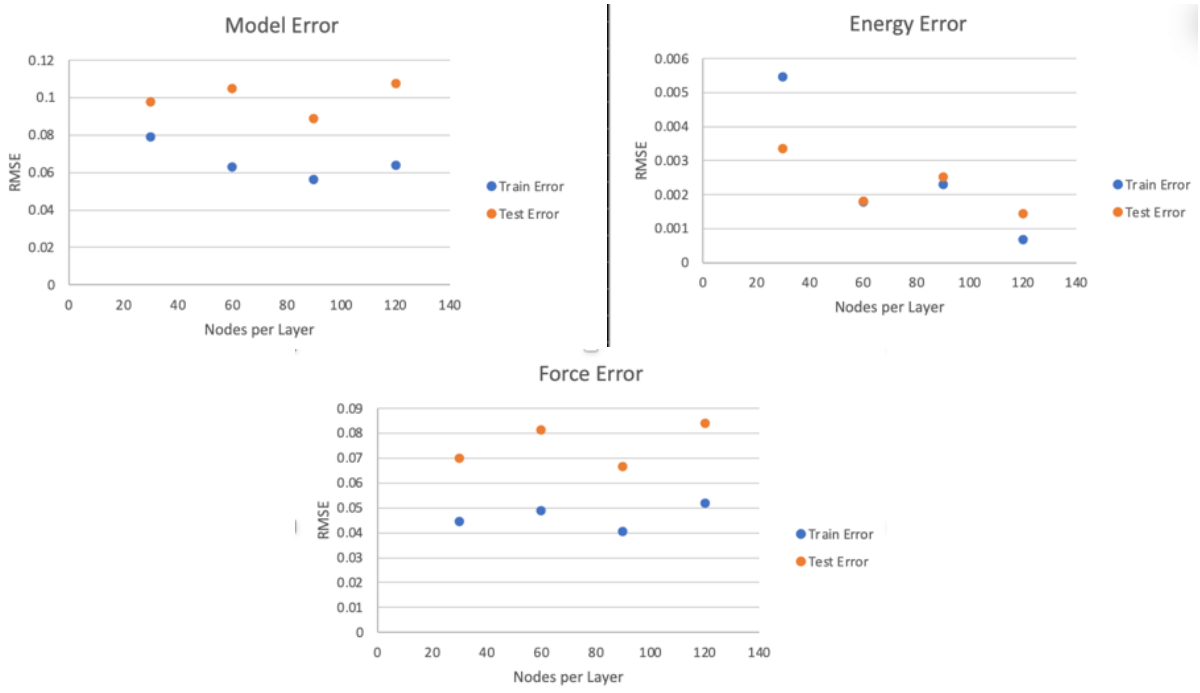

Figure 3.1: Plots for various RMSE values vs nodes per layer at a layer count of 3 layers.

The choice of nodes and hidden layers was justified by running tests using different model parameters and seeing which ones reported the lowest RMSE values. RMSE values for overall model performance, energy, and force were reported and can be seen in Figure 3.1. This test was also repeated for number of hidden layers while holding the nodes per layer constant. The results in Figure 3.1 and of the other tests all showed that model and force error were minimized at 3 hidden layers of 90 nodes each, while energy was always minimized at 5 layers with 120 nodes each. This was also verified by generating phonon dispersion curves which will be discussed in more detail in the results section.

Lastly, the potential was smoothed from an initial cutoff of 5 angstroms to a potential value of 0 by 5.4 angstroms. The original system run using VASP was a 64-atom cube of Silicon with dimensions of 10.86 angstroms, or two unit cells. Since the cutoff radius should be less than half the simulation box, the cutoff smoothed from 5 to 5.4 angstrom was chosen.

3.4 Model Validation

The developed NNP was validated in two ways: phonon dispersion compared to experiment, and thermal conductivity calculations using NEMD. For phonon dispersion curves, the program latgen was employed to generate the diamond structure for Silicon using the appropriate primitive cell dimensions [30]. The phonon data was generated in LAMMPS using the fix phonon command [31]. Post processing of phonon data was handled by the program phana [32].

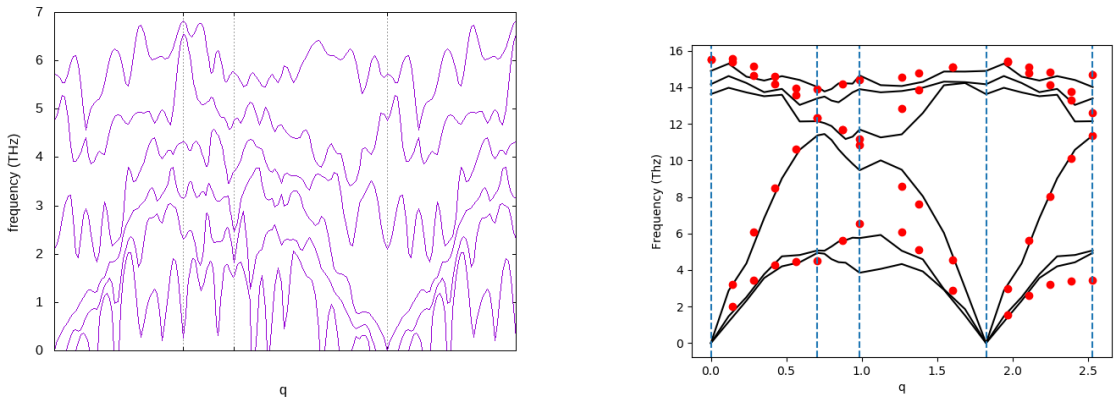

(a) (b)

Figure 3.2: (a) Phonon dispersion for Si using 3x90 NNP. (b) Black lines are phonon dispersion generated by MD using 5x120 NNP, red dots are experimental data taken from ref [33].

First, we show in Figure 3.2 that the choice of a 5x120 neural network was appropriate. As can be seen, the phonon dispersion generated by the 5x120 network matches closely with experiment, whereas the 3x90 network does not appear to be reasonable. Second, we compare the 5x120 phonon dispersion with both experimental data and the Tersoff potential (specifically Si(D) in SiCGe.tersoff) in Figure 3.3. This figure shows that again, our potential has good agreement with experimental data, but that it also outperforms the Tersoff potential in terms of accuracy.

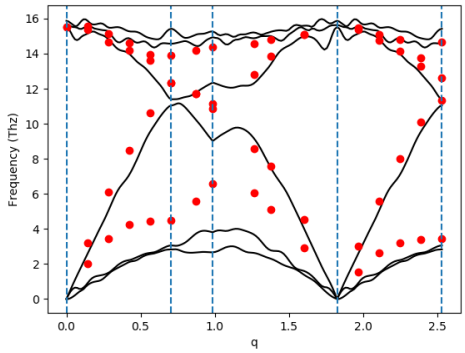

Figure 3.3: Black lines are phonon dispersion generated by MD using Tersoff potential, red dots are experimental data taken from ref [33].

Thermal conductivity calculations, however, are not as promising. The accepted thermal conductivity for bulk Silicon at 300K is approximately 148 W/mK [34]. The value reported by the NNP is approximately 30 W/mK which is much lower. Improvement is possible, however, upon running more simulations it was discovered that there was some trouble with equilibration when using the NNP, and results did improve slightly after that was increased. With more appropriate equilibration it is expected the NNP will perform as intended. The drawback is that the model performance is now approaching the computational expense of *ab-initio* MD for the same domain size, when it should run closer to the speeds of classical MD.

3.5 Discussion

Results for the NNP for bulk Silicon are promising in the sense that the phonon dispersion curve was accurately reproduced and was in excellent agreement with experiment. The model has been generated again using the 4x4x4 K-grid, which reproduced the phonon dispersion curves just

as well, but did not show improvement in thermal conductivity calculations. The issue persists in equilibration during MD, with NVT and NPT equilibration running smoothly. However, under NVE conditions as well as NEMD thermostatted conditions, the system no longer behaves as expected. Despite adequate equilibration under NVT and NPT, the system explodes and consequently fails once NVE is initiated for the 4x4x4 grid. This issue does not present itself as much for the 3x3x3 grid, however. Under NEMD conditions for the 3x3x3 grid, the thermosetting does not work as expected. The thermostatting for the hot and cold regions is expected to return energy values opposite in sign and equal in magnitude for energy added to the hot and energy subtracted from the cold. However, we show a discrepancy in these values, which is a contributing factor in the miscalculated thermal conductivity.

4. CONCLUSIONS AND FUTURE WORK

The lower limits of thermal conductivity sought to exist for SL and RML structures has successfully been broken. Using a Genetic Algorithm optimization method, an RML structure of Si and Ge was found that reduces thermal conductivity to approximately 1 W/mK. This result is important for the applications of SL and RML structures, not just of SiGe, but for other materials commonly used in thermoelectric energy generation such as bismuth-telluride.

The NNP generated for bulk Silicon was able to successfully replicate the phonon dispersion curves for Silicon. This shows the potential can match experimental accuracy and outperform the classical Tersoff potential. The thermal conductivity issues remain to be solved, though it is believed that more accurate DFT data and longer MD equilibration will produce accurate results. For future work, this NNP needs to be expanded to Aluminum and the Silicon-Aluminum interface. The framework for generating the model and generating data is in place and semi-automated, so the work may proceed with relative ease once the Silicon model has been fully validated.

APPENDIX A. DEEPMD INPUT FILE

```
{
    "model":{
        "type_map": ["Si"],
        "data_stat_nbatch": 15,

        "descriptor":{
            "type": "se_a",
            "sel": [50],
            "rcut":  5.00,
            "rcut_smth": 5.40
        },
        "fitting_net":{
            "type": "ener",
            "neuron": [120,120,120,120,120],
            "activation_function": "tanh",
            "seed": 5
        }
    },
    "loss":{
        "type": "ener"
    },
    "learning_rate":{
        "type": "exp"
    },
    "training":{
        "systems": "../../data_compiled/",
        "set_prefix": "set",
        "stop_batch": 100000,
        "batch_size": "auto",
        "seed": 1,
        "disp_file": "lcurve.out",
        "disp_freq": 100,
        "save_freq": 100,
        "save_ckpt": "model.ckpt",
        "disp_training": true,
        "time_training": true
    }
}
```

APPENDIX B. SAMPLE LAMMPS SCRIPT FOR NEMD

```
#### NEMD script for bulk Si

## Initialize

units metal
dimension 3
boundary p p p
atom_style atomic

## System

lattice diamond 5.4307 orient x 1 0 0 orient y 0 1 0 orient z 0 0 1
region sim block 0 40 0 5 0 5
create_box 1 sim
create_atoms 1 region sim
mass 1 28.0855

variable        l_c equal 5.4307
variable        NRML equal 20
variable        Nleftright equal 20
variable        Nedge equal 1
variable        Nres equal 9

variable        Neach equal ${NRML}+${Nleftright}
variable        posi_leftedge equal ${Nedge}*${l_c}-0.1
variable        posi_rightedge equal (${Neach}-${Nedge})*${l_c}-0.1
variable        posi_hot equal (${Nedge}+${Nres})*${l_c}-0.1
variable        posi_cold equal (${Neach}-${Nedge}-${Nres})*${l_c}-0.1
```

```
region          112 block INF ${posi_leftedge} INF INF INF INF units box
group           edge_left region 112
region          113 block ${posi_rightedge} INF INF INF INF INF units box
group           edge_right region 113
region          114 block ${posi_leftedge} ${posi_rightedge} INF INF INF INF units box
group           mid region 114

region          2 block ${posi_leftedge} ${posi_hot} INF INF INF INF  units box
group           hot region 2
region          3 block  ${posi_cold} ${posi_rightedge} INF INF INF INF  units box
group           cold region 3

## Simulation Settings

pair_style deepmd graph.pb
pair_coeff
timestep 0.001

## Equilibration

velocity all create 300.0 821745 mom yes rot yes dist gaussian

fix fxmom all momentum 1 linear 1 1 1 angular

fix 1 all nvt temp 300.0 300.0 0.05
thermo_style custom step temp ke pe etotal press lx ly lz
thermo 1000

run 50000

unfix 1
```

```
fix 2 all npt temp 300.0 300.0 0.05 iso 0.0 0.0 0.5

run 50000

unfix 2
fix 3 all nve

run 50000

write_data equil.data
unfix 3
unfix fxmom

## NEMD

velocity edge_left set 0.0 0.0 0.0
velocity edge_right set 0.0 0.0 0.0
fix fxleft edge_left setforce 0.0 0.0 0.0
fix fxright edge_right setforce 0.0 0.0 0.0

fix fxhot hot langevin 330.0 330.0 0.05 821745 tally yes
fix fxcold cold langevin 270.0 270.0 0.05 821745 tally yes
fix 6 mid nve

compute temp_hot hot temp
compute temp_cold cold temp

thermo_style custom step temp ke pe etotal press vol c_temp_hot c_temp_cold f_fxhot f_fxcold
thermo 10000

run 300000
```

```
## Final run
reset_timestep 0
variable myLx equal lx
variable myLy equal ly
variable myLz equal lz

compute cc1 all chunk/atom bin/1d x lower 1.3575 units box
fix 105 all ave/chunk 10 10000 100000 cc1 temp file Tgrad.txt
fix fluxout all ave/time 1 1 1000 v_myLy v_myLz f_fxhot f_fxcold file fluxout.txt

run 1000000
```

REFERENCES

[1]. *Department of Physics*. Phonons. (n.d.). https://warwick.ac.uk/fac/sci/physics/current/postgraduate/regs/mpagswarwick/ex5/phonons/.

[2]. Wang, Y., Huang, H., & Ruan, X. (2014). Decomposition of coherent and incoherent phonon conduction in superlattices and random multilayers. *Physical Review B*, *90*(16). https://doi.org/10.1103/physrevb.90.165406

[3]. Pappas, S. (2018, April 27). *Facts About Silicon*. LiveScience. https://www.livescience.com/28893-silicon.html.

[4]. LAMMPS Molecular Dynamics Simulator. (n.d.). https://www.lammps.org/.

[5]. Lammps. (2020, June 14). *lammps/lammps*. GitHub. https://github.com/lammps/lammps/blob/master/potentials/SiCGe.tersoff.

[6]. B. Jelinek, S. Groh, M.F. Horstemeyer, J. Houze, S.G. Kim, G.J. Wagner, A. Moitra, and M.I. Baskes (2012), "Modified embedded atom method potential for Al, Si, Mg, Cu, and Fe alloys", *Physical Review B*, **85(24)**, 245102. DOI: 10.1103/physrevb.85.245102.].

[7]. The Trustees of Princeton University. (n.d.). *nglos324 - potential*. Princeton University. https://www.princeton.edu/~maelabs/mae324/glos324/potential.htm.

[8]. Abs da Cruz, C., Termentzidis, K., Chantrenne, P., & Kleber, X. (2011). Molecular dynamics simulations for the prediction of thermal conductivity of bulk silicon and silicon nanowires: Influence of interatomic potentials and boundary conditions. *Journal of Applied Physics*, *110*(3), 034309. https://doi.org/10.1063/1.3615826

[9]. *pair_style tersoff command*¶. pair_style tersoff command - LAMMPS documentation. (n.d.). https://docs.lammps.org/pair_tersoff.html.

[10]. *compute heat/flux command*¶. compute heat/flux command - LAMMPS documentation. (n.d.). https://docs.lammps.org/compute_heat_flux.html.

[11]. Sosso, G. C., Deringer, V. L., Elliott, S. R., & Csányi, G. (2018). Understanding the thermal properties of amorphous solids using machine-learning-based interatomic potentials. *Molecular Simulation*, *44*(11), 866–880. https://doi.org/10.1080/08927022.2018.1447107

[12]. Algorithms. (2011). *Graph Coloring Problems*, 168–179. https://doi.org/10.1002/9781118032497.ch10

[13]. Bartók, A. P., & Csányi, G. (2015). Gaussian approximation potentials: A brief tutorial introduction. *International Journal of Quantum Chemistry*, *115*(16), 1051–1057. https://doi.org/10.1002/qua.24927

[14]. Rowe, P., Csányi, G., Alfè, D., & Michaelides, A. (2018). Development of a machine learning potential for graphene. *Physical Review B*, *97*(5), 054303.

[15]. Behler, J. (2011). Atom-centered symmetry functions for constructing high-dimensional neural network potentials. *The Journal of Chemical Physics*, *134*(7), 074106. https://doi.org/10.1063/1.3553717

[16]. Behler, J., & Parrinello, M. (2007). Generalized Neural-Network Representation of High-Dimensional Potential-Energy Surfaces. *Physical Review Letters*, *98*(14). https://doi.org/10.1103/physrevlett.98.146401

[17]. Dziubek, M. (2019, November 10). *Let me introduce you to neural networks*. Medium. https://towardsdatascience.com/let-me-introduce-you-to-neural-networks-fedf4253106a.

[18]. Sanville, E., Bholoa, A., Smith, R., & Kenny, S. D. (2008). Silicon potentials investigated using density functional theory fitted neural networks. *Journal of Physics: Condensed Matter*, *20*(28), 285219. https://doi.org/10.1088/0953-8984/20/28/285219

[19]. *DeePMD-kit*. DeePMDkit. (n.d.). http://www.deepmd.org/.

[20]. Wang, H., Zhang, L., Han, J., & Weinan, E. (2018). DeePMD-kit: A deep learning package for many-body potential energy representation and molecular dynamics. *Computer Physics Communications*, *228*, 178-184.

[21]. Rapier, R. (2020, June 25). *Fossil Fuels Still Supply 84 Percent Of World Energy - And Other Eye Openers From BP's Annual Review*. Forbes. https://www.forbes.com/sites/rrapier/2020/06/20/bp-review-new-highs-in-global-energy-consumption-and-carbon-emissions-in-2019/?sh=48f0974266a1.

[22]. Nicola Jones • May 29, Nicola Jones, Nicola Jones, •, Nicola Jones is a freelance journalist based in Pemberton, Jones →, M. about N., Fleming, P., Fleming, P., Katz, C., Katz, C., Hockenos, P., & Hockenos, P. (n.d.). *Waste Heat: Innovators Turn to an Overlooked Renewable Resource*. Yale E360. https://e360.yale.edu/features/waste-heat-innovators-turn-to-an-overlooked-renewable-resource.

[23]. shahadalsudais, A. (2016, February 29). *Thermoelectric Devices: What They Are & Examples*. Scientific Thoughts. https://sites.suffolk.edu/shahadalsudais/2016/02/29/thermoelectric-devices-what-they-are-examples/.

[24]. Snyder, G. J., & Snyder, A. H. (2017). Figure of merit ZT of a thermoelectric device defined from materials properties. *Energy & Environmental Science*, *10*(11), 2280–2283. https://doi.org/10.1039/c7ee02007d

[25]. *fix langevin command*¶. fix langevin command - LAMMPS documentation. (n.d.). https://docs.lammps.org/fix_langevin.html.

[26]. Chowdhury, P. R., Reynolds, C., Garrett, A., Feng, T., Adiga, S. P., & Ruan, X. (2020). Machine learning maximized Anderson localization of phonons in aperiodic superlattices. *Nano Energy*, *69*, 104428.

[27]. Prabudhya Roy Roy Chowdhury, Adam Sandor Garrett, Colleen Reynolds, Xiulin Ruan (2018), "Simulation based Thermal Design Framework for Accelerated Structure exploration (STEDFAST)," https://nanohub.org/resources/stedfast. (DOI: 10.4231/D3JS9H991).

[28]. Init.at. (n.d.). *Vienna Ab initio Simulation Package*. VASP. https://www.vasp.at/.

[29]. Wen, M., & Tadmor, E. B. (2019). Hybrid neural network potential for multilayer graphene. *Physical Review B*, *100*(19). https://doi.org/10.1103/physrevb.100.195419

[30]. Lingtikong. (n.d.). *lingtikong/latgen*. GitHub. https://github.com/lingtikong/latgen.

[31]. *fix phonon command*¶. fix phonon command - LAMMPS documentation. (n.d.). https://docs.lammps.org/fix_phonon.html.

[32]. Lingtikong. (n.d.). *lingtikong/phana*. GitHub. https://github.com/lingtikong/phana.

[33]. G. Dolling, Inelastic Scattering Neutrons Solids Liquids Proc. Symp. 2nd Chalk River, Can. 1962 (1963), p. 37.

[34]. *Properties of silicon and silicon wafers*. El. (n.d.). https://www.el-cat.com/silicon-properties.htm.

PUBLICATIONS

1. Prabudhya Roy Roy Chowdhury, Adam Sandor Garrett, Colleen Reynolds, Xiulin Ruan (2018), "Simulation based Thermal Design Framework for Accelerated Structure exploration (STEDFAST)," https://nanohub.org/resources/stedfast. (DOI: 10.4231/D3JS9H991).

2. Chowdhury, P. R., Reynolds, C., Garrett, A., Feng, T., Adiga, S. P., & Ruan, X. (2020). Machine learning maximized Anderson localization of phonons in aperiodic superlattices. *Nano Energy*, *69*, 104428.